Frontiers of Physics
https://doi.org/10.1007/s11467-018-0831-x
Front. Phys.
14(1), 13605 (2019)

RESEARCH ARTICLE

Phase transition of the frustrated antiferromagntic J_1-J_2-J_3 spin-1/2 Heisenberg model on a simple cubic lattice

Ai-Yuan Hu[1], **Huai-Yu Wang**[2,†]

[1] *College of Physics and Electronic Engineering, Chongqing Normal University, Chongqing 401331, China*
[2] *Department of Physics, Tsinghua University, Beijing 100084, China*
Corresponding author. E-mail: [†] *wanghuaiyu@mail.tsinghua.edu.cn*
Received May 4, 2018; accepted July 14, 2018

We have comprehensively investigated the frustrated J_1-J_2-J_3 Heisenberg model on a simple cubic lattice. This model allows three regimes of magnetic order, viz., (π,π,π), $(0,\pi,\pi)$ and $(0,0,\pi)$, denoted as AF1, AF2, and AF3, respectively. The effects of the interplay of neighboring couplings on the model are studied in the entire temperature range. The zero temperature magnetic properties of this model are discussed utilizing the linear spin wave (LSW) theory, nonlinear spin wave (NLSW) theory, and Green's function (GF) method. The zero temperature phase diagrams evaluated by the LSW and NLSW methods are illustrated, and are observed to exhibit different parameter boundaries. In certain regions and along the parameter boundaries, the possible phase transformations driven by the parameters are discussed. The results obtained using the LSW, NLSW, and GF methods are compared with those obtained using the series expansion (SE) method, and are observed to be in good agreement when the value of J_2 is not close to the parameter boundaries. The ground state energies obtained using the LSW and NLSW methods are close to that obtained using the SE method. At finite temperatures, only the GF method is employed to evaluate the magnetic properties, and the calculated phase diagram is observed to be identical to the classical phase diagram. The results indicate that at the parameter boundaries, a temperature-driven first-order phase transition between AF1 and AF2 may occur along the boundary line. Along the AF1-AF3 and AF2-AF3 boundary lines, AF3 is less stable than AF1 and AF2. Our calculated critical temperature agrees with that obtained using Monte Carlo simulations and pseudofermion functional renormalization group scheme.

Keywords quantized spin models, quantum phase transitions, antiferromagnetics

1 Introduction

Over the past two decades, frustrated quantum Heisenberg model with competing nearest-neighbor (NN) antiferromagnetic (AF) exchange interaction J_1 and next-nearest neighbor (NNN) J_2 has been studied extensively [1–3]. A well-known example was the quantum spin-1/2 J_1-J_2 Heisenberg model (known as the J_1-J_2 model) on a square lattice, which has been investigated by various methods. Their critical properties were well known [4–22]. In the absence of the NNN interactions, the ground state is antiferromagnetically ordered. The presence of the NNN interactions is expected to induce strong frustration and may strongly affect the AF order. It was believed that at zero temperature the competition between the J_1 and J_2 leads to a disordered quantum spin-liquid at $0.4 < J_2/J_1 < 0.6$ [13, 20, 21]. For $J_2/J_1 \leq 0.4$, the system was a Néel state (AF1), and for $J_2/J_1 \geq 0.6$ it turned to be a collinear state (AF2). The quantum phase transition from the AF1 to the spin liquid state at $J_2/J_1 = 0.4$ was of the second order, while the transition from the spin liquid state to AF2 at $J_2/J_1 = 0.6$ was of the first order one.

Recently various methods have been used to explore the critical properties of the three-dimensional J_1-J_2 frustrated model on a simple cubic lattice. These methods included the linear spin wave theory (LSW) [23], the nonlinear spin wave theory (NLSW) [23], a spherically symmetric Green function [24], the couple-cluster method (CCM) [25], the effective field approach [26] and the Monte Carlo simulations (MCS) [27]. These investigations showed that there were two possible states, i.e., the AF1 and AF2, see Figs. 1(a) and (b). When the next-next-nearest-neighbor (NNNN) exchange J_3 was induced, i.e., J_1-J_2-J_3 frustrated model, the competition between J_2/J_1 and J_3/J_1

leads to the emergence of AF3, see Fig. 1(c) [28, 29]. It indicated that the role of J_3 was important for the phase transition of this system. Generally speaking, quantum fluctuation of a simple lattice is weaker in contrast to the two-dimensional square lattice. The results based on a function renormalization prompted that a nonmagnetic phase might emerge in this model at zero temperature within a certain parameter region [28]. In the present work, we will use different theoretical methods to proceed a comprehensive investigation and try to explore possible phase transition of the spin-1/2 J_1-J_2-J_3 frustrated model on a simple cubic lattice.

2 Model and method

The Hamiltonian of the spin-1/2 J_1-J_2-J_3 Heisenberg frustrated model on a simple cubic lattice reads

$$H = J_1 \sum_{\langle i,j \rangle} S_i \cdot S_j + J_2 \sum_{\ll i,j \gg} S_i \cdot S_j + J_3 \sum_{[i,j]} S_i \cdot S_j. \quad (1)$$

where the three summations are over the pairs of each spin with its first-, second-, and third-nearest neighbors in the cubic lattice, respectively, and the S_i is quantum spin-1/2 operator. The J_1, J_2 and J_3 are exchange parameters, and all of them are assumed to be positive (antiferromagnetic). We set $J_1 = 1$, which also sets an energy scale.

The three possible phases or states are sketched in Fig. 1, and can be labeled by their ordering vectors (π, π, π), $(0, \pi, \pi)$ and $(0, 0, \pi)$, respectively. In each phase, the lattice is divided into two sublattices, and since we do not consider external magnetic field, the absolute values of the two sublattice magnetizations, denoted as m, are the same. In the AF1 phase, the J_2 interaction is frustrating while the J_3 interaction strengthens the order. In the other phases the J_1 and J_2 are partially frustrating, while J_3 strengthens the frustration in the AF2, but does not so in the AF3.

The motivation for the present work is to investigate the zero and finite temperature phases of this model by different theoretical techniques and to explore the effect of the interplay of neighboring couplings on the possible phase transition of this model. For the case of zero temperature, we use the LSW [30], NLSW [31] and double-time Green's function (GF) method [32]. The results obtained from different methods will be compared to each other. For finite temperature, only the GF is adopted [32]. The formalisms of these three theoretical methods are lengthy. We introduce them with some details in the appendix, taking the AF1 configuration as an example.

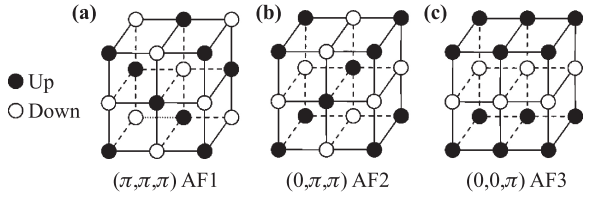

Fig. 1 Illustration of the three magnetic orders. Their ordering vectors are (π, π, π), $(0, \pi, \pi)$ and $(0, 0, \pi)$ which are denoted as AF1, AF2 and AF3 states, respectively. Solid and open symbols represent "up" and "down" spins.

Table 1 The energy E_0 and sublattice magnetization m in the case of $J_2 = J_3 = 0$ computed by various methods.

	$-E_0$	m
CCM (Ref. [25])	0.9024	0.4203
SE (Ref. [29, 33])	0.9021	0.424
TOSW (Ref. [33])	0.9025	0.4227
ED (Ref. [25])	0.9314	
LSW (This work, Ref. [23])	0.8957	0.4216
NLSW (This work, Ref. [23])	0.9028	0.4216
GF (This work)	0.8675	0.4158

3 Results and discussion

3.1 Zero temperature

3.1.1 Magnetic properties

In this section, the LSW, NLSW and GF methods are used to calculate the magnetic properties of the system, and the results will be compared to other methods, mainly series expansion (SE).

First of all, let us see the simplest case where $J_2 = J_3 = 0$. Recently, some theoretical methods gave the values of ground state energy E_0 and sublattice magnetization m in this case. These values are listed in Table 1 for comparison. Generally, the result of the SE up to the 12^{th} order was believed reliable. It is seen that the E_0 by the NLSW is in good agreement with those by the SE, CCM and third-order spin-wave (TOSW) theory. The result of exact diagonalization (ED) deviates slightly from the above four methods. The reason may be that the size of the lattice treated is relatively small in the ED calculation [25]. Comparison of the LSW with NLSW and TOSW results indicates that the high-order corrections are significant. It is easily understood that the NLSW considers the interactions between the spin waves, so that brings some corrections to the LSW which only considers the noninteracting spin waves. Nevertheless, the magnetization m evaluated by different methods agrees with each other. At zero temperature, the value obtained by the GF method is not so good as those by other methods.

Figure 2 plots the ground state energies E_0 and sublattice magnetizations m of the AF1 and AF3 as functions of J_2 for $J_3 = 0.3$ and 0.6. Hereafter in all the following figures the results from the LSW, NLSW and GF methods are respectively plotted by dash-dotted, solid and dashed lines. The $E_0's$ are plotted in Figs. 2(a) and (b).

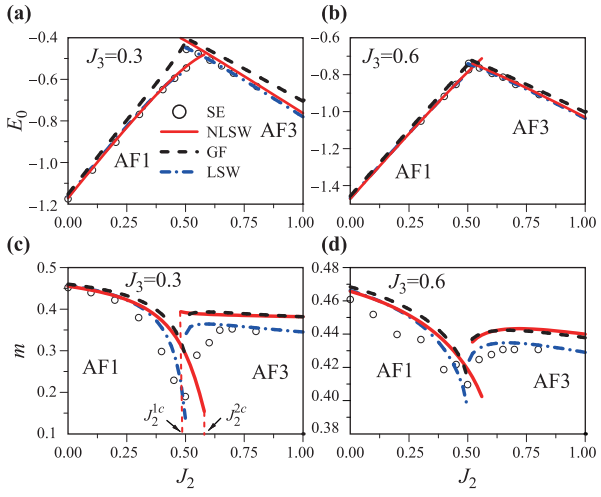

Fig. 2 Ground-state energies and sublattice magnetizations of the AF1 and AF3 as a function of J_2. **(a)** Ground-state energies at $J_3 = 0.3$. **(b)** Ground-state energies at $J_3 = 0.6$. **(c)** Magnetizations at $J_3 = 0.3$. **(d)** Magnetizations at $J_3 = 0.6$. The open circles are the SE results, and the dashed-dotted, solid and dashed lines represent the LSW, NLSW and GF results, respectively.

At $J_3 = 0.3$, the results calculated by the LSW, NLSW and SE methods are quite in agreement with each other. The GR method gives a slightly higher energy values. At $J_3 = 0.6$, the results calculated by all the four methods are almost identical. This demonstrates that the LSW, NLSW and SE methods are reliable. At $T = 0$, the GR method is not so good as the other three methods, but at certain parameters gives correct results.

The sublattice magnetization $m's$ are plotted in Figs. 2(c) and (d). When the J_2 value is small, the sublattice magnetizations evaluated by the four methods are coincide with each other, similar to the case in Table 1. While for large J_2 values, the results obtained by the LSW agree with those by the SE [29]. According to the GF and LSW, $J_2 = 0.5$ is the parameter boundary between the AF1 and AF3 phases, as $J_3 \geq 0.25$. That is to say, when $J_2 \leq 0.5$ and $J_2 \geq 0.5$, it is the AF1 and AF3, respectively, as long as $J_3 \geq 0.25$. For the NLSW, when $J_3 \geq 0.3$, it is the AF1 and AF3 for $J_2 \leq J_2^{2c}$ and $J_2 \geq J_2^{1c}$, respectively. In the region $J_2^{1c} \leq J_2 \leq J_2^{2c}$, either state is possible to exist. By contrast, near $J_2 = 0.5$ the SE method gave a narrow paramagnetic intermediate phase without long-range magnetic order [29].

Figure 3 shows the E_0 and m of AF1 and AF2 as a function of J_2 for $J_3 = 0$ and 0.15. The ground state energies are plotted in Figs. 3(a) and (b). A conclusion similar to Fig. 2 is drawn, i.e., the results calculated by the LSW, NLSW and SE methods are quite in agreement with each other, and the GR method gives energy values slightly lifted up. The parameter boundary between the AF1 and AF2 depends on the J_3 value. When $J_3 = 0$, the LSW reveals a nonmagnetic intermediate phase as $0.241 < J_2 < 0.251$. In contrast, the CCM method gave the nonmagnetic intermediate phase within the range $0.2745 < J_2 < 0.2795$ [25]. But the GF method tells that the $J_2 = 0.25$ is the clear boundary. As $J_3 = 0.15$, the parameter boundary is at $J_2 = 0.4$.

Figure 4 shows the E_0 and m of the AF2 and AF3 as a function of J_3 for $J_2 = 0.6$ and 0.8. The parameter boundary determined by the GF and LSW methods is at $J_3 = 0.25$ when $J_2 \geq 0.5$. In this case, the results of the GF method are satisfactorily coincide with those of the other three methods [29]. Other features in Fig.4 are the same as those in Figs. 2 and 3.

3.1.2 *Possible phase transition*

At zero temperature, when we say phase transition, we mean the quantum phase transition driven by parameters.

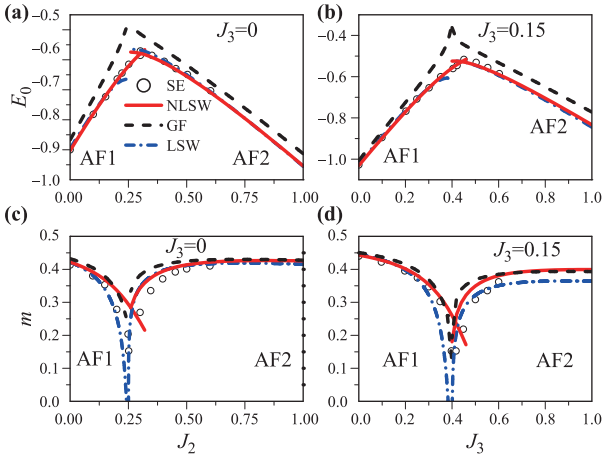

Fig. 3 Ground-state energies and magnetizations of the AF1 and AF2 as functions of J_2. **(a)** Ground-state energies at $J_3 = 0$. **(b)** Ground-state energies at $J_3 = 0.15$. **(c)** Magnetizations at $J_3 = 0$. **(d)** Magnetizations at $J_3 = 0.15$.

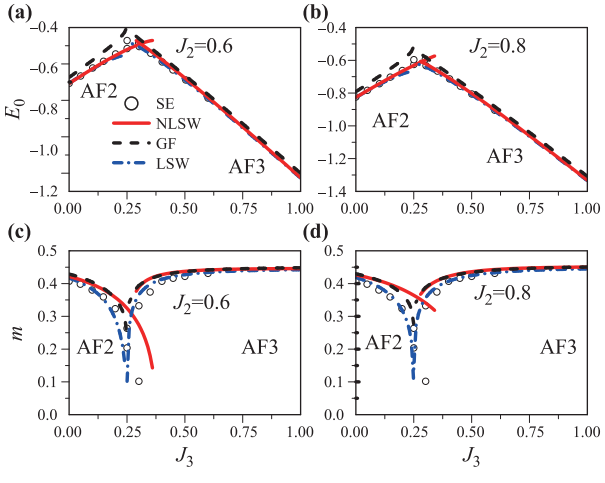

Fig. 4 Ground-state energies and magnetizations of the AF2 and AF3 as a function of J_3. **(a)** Ground-state energies at $J_2 = 0.6$. **(b)** Ground-state energies at $J_2 = 0.8$. **(c)** Magnetizations at $J_2 = 0.6$. **(d)** Magnetizations at $J_2 = 0.8$.

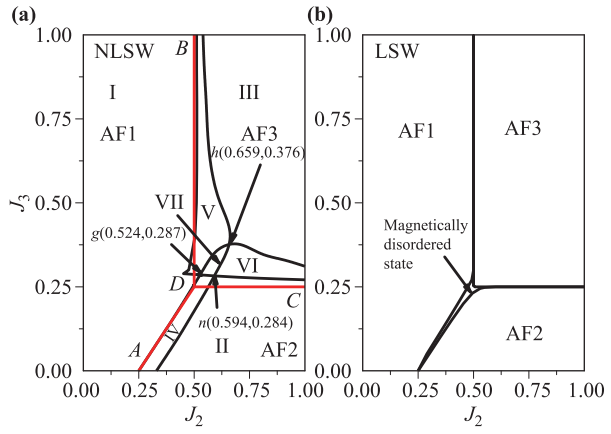

Fig. 5 Ground-state phase diagram in the (J_2, J_3) plane. **(a)** The diagram computed by the NLSW is drawn by black lines. There are seven regions. The regions I, II and III represent AF1, AF2 and AF3, respectively. IV, V and VI represent the overlap regions of AF1-AF2, AF1-AF3 and AF2-AF3, respectively. The region VII is the overlap of all the three phases, the (J_2, J_3) values of the three vertices of which are $A(0.524, 0.287)$, $B(0.659, 0.376)$ and $C(0.594, 0.284)$, respectively. The classical diagram is drawn by red lines. The three straight lines distinguish the AF1, AF2 and AF3 phases. The four end points are $A(0.25, 0)$, $B(0.5, 1)$, $C(1, 0.25)$ and $D(0.5, 0.25)$, respectively. **(b)** The diagram computed by the LSW. It contains four regions, i.e., AF1, AF2, AF3 and a region with no long-range magnetic order.

The black lines in Fig. 5(a) are the phase diagram of the ground state computed by the NLSW method. The diagram is divided into seven regions. The regions I, II and III represent AF1, AF2 and AF3, respectively. The regions IV, V and VI respectively represent the overlap of AF1-AF2, AF1-AF3 and AF2-AF3. In each overlap region, two or more phases are possible. For example, in region IV in Fig. 5(a), with the same exchange parameters, both the AF1 and AF2 phases can be calculated, but there is no AF3 long-range order. The region VII is overlap of the AF1, AF2 and AF3, i.e., the system may be any of the three phases. Figure 5(b) is the phase diagram obtained from the LSW. It is divided into four regions. They are respectively the AF1, AF2, AF3 and a region with no long-rang magnetic order which is probably a spin liquid state. The GF method gives the phase diagram merely containing AF1, AF2 and AF3, which is the same as the classical one and is represented by the red lines in Fig. 5(a). Since in the overlap regions and along the parameter boundaries, more than one state with the same parameters are possible, there brings a question that which one of them is stabler. In the following, we manage to answer this question.

The specific steps are as follows. In the overlap region and along the parameter boundaries, we evaluate the ground energies of the possible phases for all possible parameters. The energies of the states AF1, AF2 and AF3 are denoted by $E_{\rm AF1}$, $E_{\rm AF2}$ and $E_{\rm AF3}$, respectively. At zero temperature, the state with a lower energy is more stable.

Figure 6 plots the energies of the three states as functions of J_2 for different J_3 values in region VII in Fig. 5(a). With the J_2 increasing, the $E_{\rm AF1}$ decreases and the $E_{\rm AF2}$ and $E_{\rm AF3}$ increase. Roughly speaking, as J_3 increases from 0.284 to 0.376, all the three energy curves shift downward, among which the $E_{\rm AF3}$ curve shifts most obviously.

Figure 6(a) shows that at $J_3 = 0.29$, the whole $E_{\rm AF3}$ curve is above the $E_{\rm AF2}$ curve. The $E_{\rm AF1}$ curve intersects with both the $E_{\rm AF2}$ and $E_{\rm AF3}$ curves. The J_2 values at which the $E_{\rm AF1}$ and $E_{\rm AF2}$ curves cross is denoted as J_2^1, and that at which the $E_{\rm AF1}$ and $E_{\rm AF2}$ curves cross is denoted as J_2^2. At $J_3 = 0.29$, $J_2^1 < J_2^2$. As $J_2 < J_2^1$, $E_{\rm AF1} < E_{\rm AF2} < E_{\rm AF3}$, so that the AF1 state is the most stable. As $J_2^1 < J_2$, the AF2 state is the most stable. At the point J_2^1, an AF1-AF2 phase transformation may occur. Numerical calculation shows that as long as $J_3 < 0.29$ and in the region VII, the features are the same as Fig. 6(a). As the J_2 value increases from 0.29, the J_2^1 and J_2^2 values close to each other, see Fig. 6(b). When the J_2 value increases to 0.315, the J_2^1 and J_2^2 values are the same. In this case, as $J_2 < J_2^1$, the AF1 is the most stable, and as $J_2 > J_2^1$, the AF2 is the most stable. Therefore, in this case, a phase transition between the AF1 and AF2 states may occur. As the J_3 increases from 0.315, the J_2^1 and J_2^2 values gradually separate, and $J_2^1 > J_2^2$. At $J_3 = 0.33$, the whole $E_{\rm AF3}$ curve becomes below the $E_{\rm AF2}$ curve, see Fig. 6(c). At $J_2 < J_2^2$, $E_{\rm AF1} < E_{\rm AF3} < E_{\rm AF2}$, i.e., the AF1 is still the most stable. As $J_2^2 < J_2$, $E_{\rm AF3} < E_{\rm AF1} < E_{\rm AF2}$, i.e., the AF3 is the most stable. At the cross point J_2^2, an AF1-AF3 phase transformation may occur. As the J_3 value increases further, say to about $J_3 = 0.35$, the $E_{\rm AF3}$ curve is totally below the other two curves. In this case, the AF3 is the most stable. When the $J_3 > 0.35$, the features are the same as in Fig. 6(d).

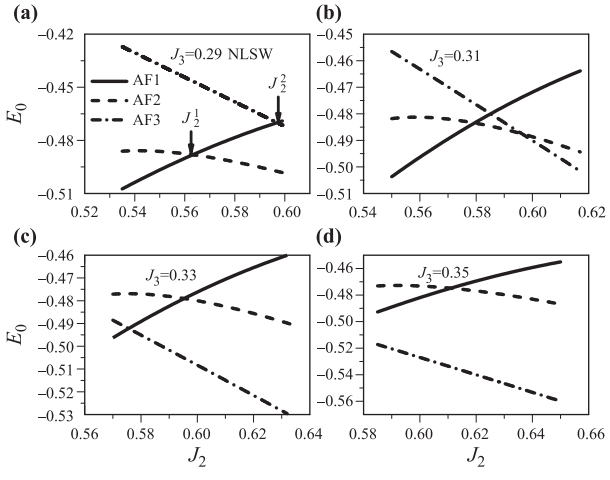

Fig. 6 Ground-state energies of the three states when the J_2 and J_3 take values in region VII of Fig. 5(a). **(a)** J_3 =0.29. **(b)** J_3 =0.31. **(c)** J_3 =0.33 and **(d)** J_3 =0.35.

The energies of both states in each of the regions IV, V and VI in Fig. 5(a) are also computed. We do not depict the energy curves as functions of parameters, but simply give the conclusions.

In region IV, the $E_{\rm AF1}$ and $E_{\rm AF2}$ as a function of J_2 for different J_3 values are calculated. They always cross. The J_2 value at the cross point is denoted as J_2^c. As $J_2 < J_2^c$, the $E_{\rm AF1} < E_{\rm AF2}$, which means that the AF1 is more stable. As $J_2 > J_2^c$, the $E_{\rm AF1} > E_{\rm AF2}$, i.e., the AF2 is more stable. At the J_2^c, an AF1-AF2 phase transformation can occur.

In region V, the $E_{\rm AF1}$ and $E_{\rm AF3}$ as a function of J_2 for different J_3 values are calculated. When the J_3 value is in the vicinity of 0.3, $E_{\rm AF1} < E_{\rm AF3}$, i.e., the AF1 is more stable. As the J_3 value increases, the two energy curves cross. The J_2 value at the cross point is again denoted as J_2^c. As $J_2 < J_2^c$, $E_{\rm AF1} < E_{\rm AF3}$, AF1 is more stable. As $J_2 > J_2^c$, $E_{\rm AF1} > E_{\rm AF3}$, so that the AF3 is more stable. At the cross point, a phase transition between AF1 and AF3 states may occur.

In region VI, the $E_{\rm AF2}$ and $E_{\rm AF3}$ as a function of J_2 for different J_3 values are calculated. When the J_3 value is well above 0.29, the $E_{\rm AF3}$ is well below the $E_{\rm AF2}$, so that the AF3 state is always more stable. As the J_3 value lowers, the $E_{\rm AF2}$ and $E_{\rm AF3}$ curves shift downward and upward, respectively. When the J_3 closes to 0.29, the two curves intersect as the J_2 closes to 0.6. At the cross point, a phase transition between AF2 and AF3 states can occur.

Now we turn to the diagram in Fig. 5(b). Numerical computation leads to the following conclusions. Along the boundary line between the AF1 and AF3, the AF1 is always more stable. Along the boundary line between the AF2 and AF3, the AF2 is always more stable.

3.2 Finite temperature

3.2.1 Phase diagram

Figure 7 depicts the Néel temperature T_N as a function of J_2 at fixed J_3 value. Figure 7(a) shows the two cases of $J_3 = 0$ and $J_3 \neq 0$. Let us first see the case of $J_3 = 0$. As J_2 increases from 0, the competition between the J_1 and J_2 emerges and becomes stronger. It leads to the drop of the T_N. When $J_2 = 0.25$, the competition between the J_1 and J_2 is the strongest, so that the Néel temperature is zero. As the J_2 rises from 0.25, the competition becomes comparatively weaker, which leads to rise of the T_N.

When $J_3 \neq 0$, the competition between J_2 and J_3 emerges. Note that we have fixed $J_1 = 1$. For the AF1 state, as the J_3 increases from 0, the competition between the J_2 and J_3 becomes weaker, and either is the frustration of the system. It leads to rise of the T_N. The AF2 state is just a contrary case, i.e., the competition between the J_2 and J_3 becomes stronger with increasing J_3. The frustration of the system also becomes stronger, which results in the drop of the T_N. Due to these two reasons, the cross point of the T_N curves of the two states shifts rightwards with increasing J_2, see the dashed lines in Fig. 7(a). When J_3 increases to 0.25, the AF3 emerges, and the critical temperature curves of the AF2 and AF3 are exactly coincident, see Figs. 7(b) and (c). When J_3 increases from 0.25, the AF2 disappears and the T_N of the AF3 increases with the increase of J_3, see Figs. 7(b). It shows that the AF2 and AF3 phases begin to separate at $J_3 = 0.25$.

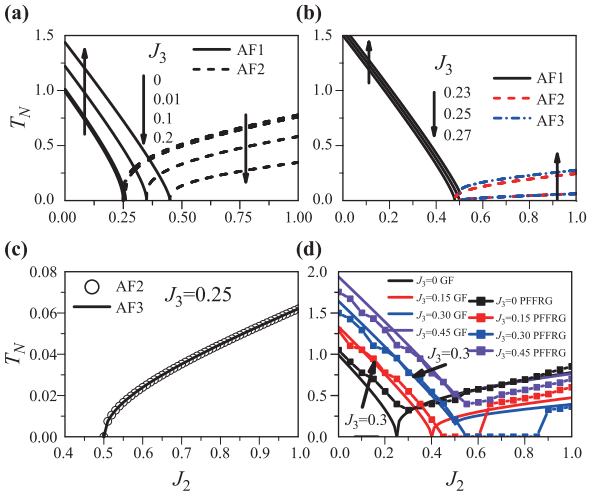

Fig. 7 The Néel temperatures T_N of the three states as a function of J_2 at different J_3 values. **(a)** $J_3 = 0$, 0.01, 0.1 and 0.2. **(b)** $J_3 = 0.23$, 0.25 and 0.27. **(c)** $J_3 = 0.25$. **(d)** $J_3 = 0$, 0.15, 0.3 and 0.45. The solid curves and solid squares represent the GF and PFFRG results. For $J_3 = 0.25$, the two curves are identical.

In Fig. 7(d), we compare the results evaluated by the GF method in this work with those by the pseudofermion functional renormalization group (PFFRG) method [28]. We discuss two cases of $J_2 \neq 0$ and $J_2 = 0$. For $J_2 \neq 0$, we plot the critical temperature as a function J_2 for different J_3 values. By the GF method, at $(J_2, J_3) = (0.25, 0)$ there can occur phase transitions between the AF1 and AF2, and at $(J_2, J_3) = (0.5, 0.45)$ there can occur phase transitions between the AF1 and AF3. By contrast, according to the PEERG method, the parameters for these two phases transitions to happen are $(J_2, J_3) = (0.3, 0)$ and $(0.55, 0)$, respectively. In light of the PFFRG method, there are parameter regions where the system has no ordered phase at nonzero temperature. These regions are $0.45 \leq J_2 \leq 0.6$ at $J_3 = 0.15$ and $0.55 \leq J_2 \leq 0.85$ at $J_3 = 0.3$, respectively [28]. While by the GF method, there is no such nonmagnetic area.

For $J_2 = 0$, we calculate the critical temperature at several J_3 values. The results are listed in Table 2. At $J_2 = 0$, the J_1 and J_3 interactions are nonfrustrating in AF1. Therefore, there is no sign problem for MCS. In this case, the result based on MCS is reliable. It is seen from Table 2 that our results are closer to MCS [34] than those of the PFFRG. And this trend is more pronounced as J_3 increases. It is worth noting that the mean-field Néel temperature $T_N = 1.5$ at $J_2 = J_3 = 0$ is too large.

Table 2 The Néel point evaluated by three methods when $J_2 = 0$.

J_3	0	0.2	0.4	0.6	0.8
PFFRG (Ref. [28])	1.05(5)	1.43(7)	1.67(8)	1.94(9)	2.36(10)
MCS (Ref. [34])	0.946(1)	1.371(1)	1.7675(10)	2.143(1)	2.5039(5)
GF (This work)	0.9893	1.4373	1.8413	2.2231	2.5914

The diagram at finite temperature calculated by the GF method is depicted by the red lines in Fig. 5(a). It is identical to the classical one. The straight line DA is the border line between the AF1 and AF2, the line DB is that between the AF1 and AF3, and the line DC between the AF2 and AF3.

Figure 8 plots the Néel points along these three red boundary lines in Fig. 5(a). Along each boundary line, the two phases have exactly the same T_N values under the same parameters. Figure 8(a) shows the Néel point along the DA line. The Néel temperatures are rather low but not zero. The curve is straight, and can be expressed by $T_N = 0.00408 - 0.00816J_2$. Figures 8(b) and (c) show the Néel points along the DB and DC lines, respectively. All the three curve vary monotonically, and at point D, the Néel point is zero.

3.2.2 Possible phase transition

Under finite temperature, when we say phase transition, we mean the phase transition driven by temperature under fixed parameters.

On each red boundary line, i.e., DA, DB and DC lines in Fig. 5(a), the two neighboring phases are possible since their Néel points are identical, as shown in Fig. 8. Therefore, there is also an issue about which phase is more stable. The three configurations are different from each other, and their entropies at a fixed temperature are different. Therefore, the internal energy cannot be used to determine which one is more stable at finite temperature. Under the same volume and temperature, the state with lower free energy is more stable.

The free energy $F(T)$ can be evaluated numerically by means of the internal energy $E(T)$ via $F(T) = E(0) - T\int_0^T \frac{E(T')-E(0)}{T'^2}\mathrm{d}T'$, where $E(T)$ is defined as the thermostatistical average of Hamiltonian, $E = \frac{\langle H\rangle}{N}$ [32]. Computing the internal energy involves the calculation of the transverse ($\sum_{i,j}\langle S_i^+ S_j^-\rangle$) and longitudinal ($\sum_{i,j}\langle S_i^z S_j^z\rangle$) correlation functions. We do not present the lengthy derivation. Please refer to Ref. [35].

In this section, we will discuss the possible phase transition of the system at finite temperature when the parameters are along the red boundary lines in Fig. 5(a). The internal and free energies as functions of temperature for the three phases are denoted by $E_{\mathrm{AF1}}(T)$, $E_{\mathrm{AF2}}(T)$, $E_{\mathrm{AF3}}(T)$, $F_{\mathrm{AF1}}(T)$, $F_{\mathrm{AF2}}(T)$ and $F_{\mathrm{AF3}}(T)$, respectively.

Figure 9 shows the internal energies $E(T)$ and free energies $F(T)$ of the AF1 and AF2 when the J_2 and J_3 take values along the AD line in Fig. 5(a). In Fig. 9(a), the curves are for $J_2 = 0.25$ and $J_3 = 0$, i.e., point A in Fig. 5(a). The $F_{\mathrm{AF1}}(T)$ and $F_{\mathrm{AF2}}(T)$ cross at a nonzero temperature T_1. Below the T_1, $F_{\mathrm{AF1}}(T) < F_{\mathrm{AF2}}(T)$. It means that the AF1 is more stable. Above the T_1, $E_{\mathrm{AF1}}(T) > E_{\mathrm{AF2}}(T)$, i.e., the AF2 is stabler until the Néel point T_N. There can occur an AF1-AF2 phase transition at the cross point. Because their internal energies are different at the cross point, it is a first-order transition. Figures 9(b) and (c) demonstrate the cases of $J_3 > 0$. Numerical calculations further show that as the J_2 value on the AD line is less than 0.2655, a first-order phase transition between AF1 and AF2 states may also occur. However, for $J_2 > 0.2655$, the difference between the $F_{\mathrm{AF1}}(T)$ and $F_{\mathrm{AF2}}(T)$ becomes larger with increasing J_2, and the $F_{\mathrm{AF2}}(T)$ is always less than $F_{\mathrm{AF1}}(T)$, see Figs. 9(b) and (c). In this case, the AF2 is stabler.

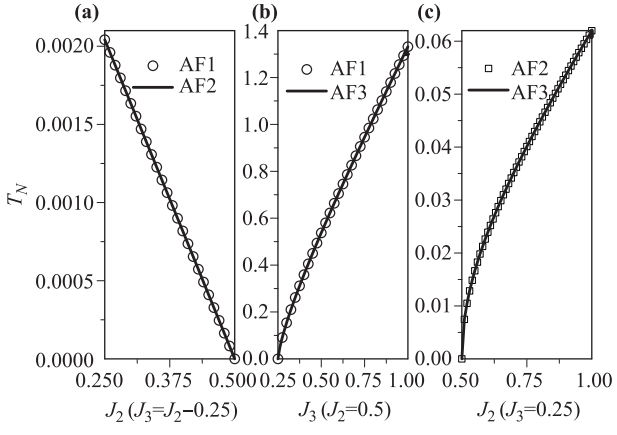

Fig. 8 The Néel temperature along the red lines **(a)** DA, **(b)** DB and **(c)** DC in Fig. 5(a). At point D, the Néel point is zero.

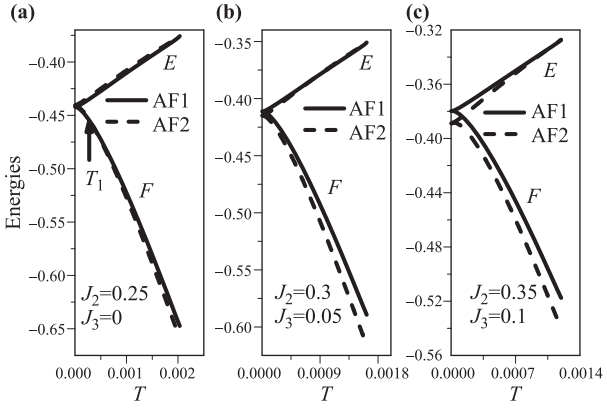

Fig. 9 The internal energies E (ascending curves) and free energies F (descending curves) of AF1 and AF2 as a functions of the temperature T when the J_2 and J_3 values are on the AD line in Fig. 5(a). **(a)** $J_2 = 0.25$ and $J_3 = 0$. **(b)** $J_2 = 0.3$ and $J_3 = 0.05$. **(c)** $J_2 = 0.35$ and $J_3 = 0.1$.

The $F_{\mathrm{AF1}}(T)$ and $F_{\mathrm{AF3}}(T)$ along the DB line in Fig. 5(a) and the $F_{\mathrm{AF2}}(T)$ and $F_{\mathrm{AF3}}(T)$ along the DC line in Fig. 5(a) are also calculated. We do not draw the curves but merely narrate the conclusions.

Along the DB line in Fig. 5(a) where $J_2 = 0.5$, the difference between the $F_{\mathrm{AF1}}(T)$ and $F_{\mathrm{AF3}}(T)$ gradually decreases as J_3 value rises. The $F_{\mathrm{AF1}}(T)$ is always less than $F_{\mathrm{AF3}}(T)$. In this case, the AF1 is always more stable. Meanwhile, the $F_{\mathrm{AF3}}(T)$ with the increase of temperature drop faster than $F_{\mathrm{AF1}}(T)$. The $F_{\mathrm{AF1}}(T)$ and $F_{\mathrm{AF3}}(T)$ curves never cross along the whole DB line in Fig. 5(a), since the former is always entirely below the latter.

Along the DC line in Fig. 5(a) where J_3=0.25. The $F(T)$ difference between the $F_{\mathrm{AF2}}(T)$ and $F_{\mathrm{AF3}}(T)$ gradually decreases as J_2 value rises. Along the whole DC line, i.e., when J_2 increases from 0.5 to 1, the $F_{\mathrm{AF2}}(T)$ is always less than $F_{\mathrm{AF3}}(T)$, and they never cross. Thus, the AF2 phase is more stable.

4 Concluding remarks

In this paper, we have studied comprehensively the J_1-J_2-J_3 Heisenberg model on a simple cubic lattice. The effects of the interplay of neighboring couplings on the magnetic properties are discussed.

At zero temperature, the LSW, NLSW and GF methods are employed to investigate the ground states, and the results are compared to the SE method. The results obtained by the LSW and NLSW methods are always close to those by the SE method. The ground state phase diagrams obtained by NLSW and LSW methods are presented. The former is divided into seven regions and the latter is divided into four. The parameter boundary lines in the LSW phase diagram expand to be coexistence regions in the NLSW phase diagram. In the overlap regions and along the boundary lines, more than one phase are possible, and under appropriate parameter rations, phase transformations driven by the parameters may occur. All the mentioned possible phase transitions are first-order one because different configurations have different entropies.

In the LSW phase diagram, along the boundary line between the AF1 and AF3, the AF1 phase is always more stable, and along that between the AF2 and AF3, the AF2 is always more stable. Therefore, along the boundary lines, there is no parameter-driving phase transition. In this phase diagram, there is a region where there is no long-range magnetic order. This region may still be short-range magnetically ordered such as a spin liquid.

At finite temperature, only GF method is used to investigate the magnetic properties. The phase diagram obtained is the same as the classical one. In the phase diagram, there are three regions, labeled by the AF1, AF2 and AF3, respectively. On each boundary line, both phases are possible, and their Néel points are always the same as long as the parameters are the same. Along the AF1-AF3 boundary line, the AF1 phase is always more stable, and along AF2-AF3 boundary line, the AF2 is always more stable. These features seem similar to those in the LSW ground state phase diagram. On the AF1-AF2 boundary line, as $0.2655 < J_2 < 0.5$, the AF2 is more stable, and as $0.25 \leq J_2 \leq 0.2655$, a phase transformation between the AF1 and AF2 driven by temperature may occur.

Acknowledgements This work was supported by the 973 Project of China (Grant No. 2012CB927402) and the Foundation for the Creative Research Groups of Higher Education of Chongqing (No. CXTDX201601016).

Appendix

In the appendix, we will present the formalisms of the LSW, NLSW and GF methods for the AF1 state. As having been mentioned in Section 2, the lattice is divided into two sublattices which are labeled by c and d, respectively, and the absolute values of the two sublattice magnetizations, denoted as m, are the same.

Appendix A Spin wave theory

We firstly make the Dyson–Maleev transformation [37] which gives

$$\begin{aligned}
S_{ci}^{+} &= \sqrt{2S}\left(a_{ci} - \frac{1}{2S}a_{ci}^{+}a_{ci}a_{ci}\right),\\
S_{ci}^{-} &= \sqrt{2S}a_{ci}^{+}, \quad S_{ci}^{z} = S - a_{ci}^{+}a_{ci},\\
S_{dj}^{+} &= \sqrt{2S}\left(b_{dj}^{+} - \frac{1}{2S}b_{dj}^{+}b_{dj}^{+}b_{dj}\right),\\
S_{dj}^{-} &= \sqrt{2S}b_{dj}^{+}, \quad S_{dj}^{z} = b_{dj}^{+}b_{dj} - S.
\end{aligned} \tag{A1}$$

Inserting equation (A1) into Eq. (1), we obtain a non-diagonal Hamiltonian, i.e.,

$$\begin{aligned}
H = {} & (-J_1 z_1 + J_2 z_2 - J_3 z_3)NS^2\\
& + J_1 \sum_{\langle i,j\rangle}\Big[S(a_{ci}^{+}a_{ci} + b_{dj}^{+}b_{dj} + a_{ci}b_{dj} + a_{ci}^{+}b_{dj}^{+})\\
& - \frac{1}{2}(a_{ci}^{+}a_{ci}a_{ci}b_{dj} + a_{ci}^{+}b_{dj}^{+}b_{dj}^{+}b_{dj}) - a_{ci}^{+}b_{dj}^{+}a_{ci}b_{dj}\Big]\\
& + \frac{J_2}{2}\sum_{\langle\langle i,j\rangle\rangle}\Big[S(a_{cj}^{+}a_{ci} + a_{ci}^{+}a_{cj} - a_{ci}^{+}a_{ci} - a_{cj}^{+}a_{cj})\\
& - \frac{1}{2}(a_{cj}^{+}a_{ci}^{+}a_{ci}a_{ci} + a_{ci}^{+}a_{cj}^{+}a_{cj}a_{cj}) + a_{ci}^{+}a_{cj}^{+}a_{ci}a_{cj}\Big]\\
& + \frac{J_2}{2}\sum_{\langle\langle i,j\rangle\rangle}\Big[S(b_{dj}^{+}b_{di} + b_{di}^{+}b_{dj} - b_{di}^{+}b_{di} - b_{dj}^{+}b_{dj})
\end{aligned}$$

$$-\frac{1}{2}(b_{di}^{+}b_{di}^{+}b_{di}b_{dj}+b_{dj}^{+}b_{dj}^{+}b_{dj}b_{di})+b_{di}^{+}b_{dj}^{+}b_{di}b_{dj}\Big]$$
$$+J_3\sum_{[i,j]}\Big[S(a_{ci}^{+}a_{ci}+b_{dj}^{+}b_{dj}+a_{ci}b_{dj}+a_{ci}^{+}b_{dj}^{+})$$
$$-\frac{1}{2}(a_{ci}^{+}a_{ci}a_{ci}b_{dj}+a_{ci}^{+}b_{dj}^{+}b_{dj}b_{dj})-a_{ci}^{+}b_{dj}^{+}a_{ci}b_{dj}\Big]. \tag{A2}$$

When all the quartic terms in Eq. (A2) are discarded, it is the LSW approximation, while when they are retained, it is the NLSW approximation. In the latter case, the quartic terms should be decoupled into quardratic forms in the following way [23]:

$$\begin{aligned}
&a_i^{+}a_ia_ib_j\simeq 2\langle a_i^{+}a_i\rangle a_ib_j+2\langle a_ib_j\rangle a_i^{+}a_i-2\langle a_ib_j\rangle\langle a_i^{+}a_i\rangle,\\
&a_i^{+}b_j^{+}b_j^{+}b_j\simeq 2\langle a_i^{+}b_j^{+}\rangle b_j^{+}b_j+2\langle b_j^{+}b_j\rangle a_i^{+}b_j^{+}-2\langle a_i^{+}b_j^{+}\rangle\langle b_j^{+}b_j\rangle,\\
&a_i^{+}b_j^{+}a_ib_j\simeq\langle a_i^{+}b_j^{+}\rangle a_ib_j+\langle a_ib_j\rangle a_i^{+}b_j^{+}+\langle a_i^{+}a_i\rangle b_j^{+}b_j\\
&\qquad+\langle b_j^{+}b_j\rangle a_i^{+}a_i-\langle a_i^{+}b_j^{+}\rangle\langle a_ib_j\rangle-\langle a_i^{+}a_i\rangle\langle b_j^{+}b_j\rangle,\\
&a_j^{+}a_i^{+}a_ia_i\simeq 2\langle a_i^{+}a_i\rangle a_j^{+}a_i+2\langle a_j^{+}a_i\rangle a_i^{+}a_i-2\langle a_i^{+}a_i\rangle\langle a_j^{+}a_i\rangle.
\end{aligned} \tag{A3}$$

After Fourier transformation, the Hamiltonian can be diagonalized using standard Bogoliubov transformation

$$\begin{aligned}
&a_k=\cosh\theta_k\alpha_k+\sinh\theta_k\beta_k^{+},\ a_k^{+}=\cosh\theta_k\alpha_k^{+}+\sinh\theta_k\beta_k,\\
&b_k=\cosh\theta_k\beta_k+\sinh\theta_k\alpha_k^{+},\ b_k^{+}=\cosh\theta_k\beta_k^{+}+\sinh\theta_k\alpha_k,
\end{aligned} \tag{A4}$$

where α_k and β_k are the bosonic operators. After the diagonalization, the Hamiltonian is expressed by

$$H=H_0-\sum_k A_k+\sum_k\omega_k+\sum_k\omega_k(\alpha_k^{+}\alpha_k+\beta_k^{+}\beta_k), \tag{A5}$$

where

$$\begin{aligned}
\omega_k&=\sqrt{A_k^2-B_k^2},\\
A_k&=S[J_1z_1-J_2z_2(1-\gamma_{2k})+J_3z_3],\\
B_k&=S(J_1z_1\gamma_{1k}+J_3z_3\gamma_{3k}),\\
\gamma_{1k}&=\frac{1}{3}(\cos k_x+\cos k_y+\cos k_z),\\
\gamma_{2k}&=\frac{1}{3}(\cos k_x\cos k_y+\cos k_x\cos k_z+\cos k_y\cos k_z),\\
\gamma_{3k}&=\cos k_x\cos k_y\cos k_z.
\end{aligned} \tag{A6}$$

z_1, z_2 and z_3 represent the number of NN, NNN and $NNNN$ sites, respectively. γ_{1k}, γ_{2k} and γ_{3k} are the structure factors of the lattice. N is the number of lattice sites.

According to the Bose statistics, the sublattice magnetization can be expressed as

$$m=S-\frac{1}{N}\sum_k\left(\frac{A_k}{\omega_k}-\frac{1}{2}\right). \tag{A7}$$

Under the LSW approximation, the ground state energy E_0 is expressed by

$$E_0=\frac{1}{2}(-J_1z_1+J_2z_2-J_3z_3)NS^2-\frac{1}{2}\sum_k A_k+\frac{1}{2}\sum_k\omega_k. \tag{A8}$$

For the NLSW approximation, we obtain

$$\begin{aligned}
E_0=&\frac{1}{2}(-J_1z_1+J_2z_2-J_3z_3)NS^2+\frac{1}{2}J_1z_1N(u+v_1)^2\\
&-\frac{1}{2}J_2z_2N(u-w)^2+\frac{1}{2}J_3z_3N(u+v_3)\\
&-\frac{1}{2}\sum_k A_k+\frac{1}{2}\sum_k\omega_k,
\end{aligned} \tag{A9}$$

$$\begin{aligned}
A_k=&S\Big[J_1z_1\left(1-\frac{u+v_1}{S}\right)-J_2z_2\left(1-\frac{u-w}{S}\right)(1-\gamma_{2k})\\
&+J_3z_3\left(1-\frac{u+v_3}{S}\right)\Big],\\
B_k=&S\left[J_1z_1\left(1-\frac{u+v_1}{S}\right)\gamma_{1k}+J_3z_3\left(1-\frac{u+v_3}{S}\right)\gamma_{3k}\right],
\end{aligned} \tag{A10}$$

where

$$\begin{aligned}
u&=\frac{1}{2}\left[\frac{2}{N}\sum_k\frac{A_k}{\omega_k}-1\right],\\
w&=\frac{1}{2}\left[\frac{2}{N}\sum_k\frac{\gamma_{2k}A_k}{\omega_k}\right],\\
v_1&=-\frac{1}{2}\left[\frac{2}{N}\sum_k\frac{\gamma_{1k}B_k}{\omega_k}\right],\\
v_3&=-\frac{1}{2}\left[\frac{2}{N}\sum_k\frac{\gamma_{3k}B_k}{\omega_k}\right].
\end{aligned} \tag{A11}$$

When J_3=0, our results will degrade to Eqs. (16), (17), (A.2), (A.3) and (A.4) of Ref. [23].

Appendix B The double-time Green's function method

The formalism follows the standard procedure in Refs. [32, 36]. The retarded GF's are constructed by

$$G_{ij}=\langle\langle S_i^{+};\mathrm{e}^{uS_j^z}S_j^{-}\rangle\rangle. \tag{B1}$$

Here, u is a parameter. After solving the Green's function by means of the method of equation of motion, u will be ultimately set as zero to give the expression of magnetization. In the course of derivation, the higher order Green functions appearing in the equation of motion have to be decoupled. In this paper, we apply random phase approximation to decouple the higher order GFs,

$$\langle\langle S_l^zS_i^{+};\mathrm{e}^{uS_j^z}S_j^{-}\rangle\rangle=\langle S_l^z\rangle\langle\langle S_i^{+};\mathrm{e}^{uS_j^z}S_j^{-}\rangle\rangle;l\neq i. \tag{B2}$$

After the decoupling, we obtain

$$\frac{2}{N}\sum_{k}\langle e^{uS_i^z}S_i^-S_i^+\rangle(k)=\theta(u)\phi. \tag{B3}$$

where the summation of wave vector k runs over the first Brillouin zone and

$$\theta(u)=\langle[S_i^+,e^{uS_i^z}S_i^-]\rangle. \tag{B4}$$

For u=0, $\theta(0)=2m$. Using Eqs. (B3) and (B4), we obtain

$$\phi_F=\frac{2}{N}\sum_{k}\frac{E_1}{2\sqrt{E_1^2-E_2^2}}\coth\frac{\sqrt{E_1^2-E_2^2}}{2k_BT}-\frac{1}{2}, \tag{B5}$$

where

$$\begin{aligned}E_1&=m[J_1z_1+J_2z_2(\gamma_{2k}-1)+J_3z_3],\\ E_2&=m(J_1z_1\gamma_{1k}+J_3z_3\gamma_{3k}).\end{aligned} \tag{B6}$$

Using Eqs. (B3), (B4), (B5) and the identity $\langle S_i^-S_i^+\rangle=S(S+1)-\langle S_i^z\rangle-\langle(S_i^z)^2\rangle$, the sublattice magnetization is expressed by

$$m=\frac{(\phi+1+S)\phi^{2S+1}-(\phi-S)(\phi+1)^{2S+1}}{(\phi+1)^{2S+1}-\phi^{2S+1}}. \tag{B7}$$

The Néel point is expressed by

$$\frac{k_BT_N}{S(S+1)}=\frac{m}{3}\left(\frac{2}{N}\sum_{k}\frac{E_1}{E_1^2-E_2^2}\right)^{-1}, \tag{B8}$$

References

1. C. Lacroix, P. Mendels, and F. Mila, Introduction to Frustrated Magnetism, Springer, Berlin, 2011
2. H. T. Diep, Frustrated Spin Systems, 2nd Ed., World Scientific, Singapore, 2013
3. J. Richter, J. Schulenburg, and A. Honecker, in: Quantum Magnetism, edited by U. Schollwöck, J. Richter, D. J. J. Farnell, and R. F. Bishop, Lecture Notes in Physics Vol. 645, Springer, Berlin, 2004, pp 85–153
4. L. Capriotti, F. Becca, A. Parola, and S. Sorella, Resonating Valence Bond Wave Functions for Strongly Frustrated Spin Systems, *Phys. Rev. Lett.* 87(9), 097201 (2001)
5. J. Sirker, Z. Weihong, O. P. Sushkov, and J. Oitmaa, J_1-J_2 model: First-order phase transition versus deconfinement of spinons, *Phys. Rev. B* 73(18), 184420 (2006)
6. J. Richter, N. B. Ivanov, and K. Retzlaff, On the violation of Marshall–Peierls sign rule in the frustrated J_1-J_2 Heisenberg antiferromagnet, *Europhys. Lett.* 25(7), 545 (1994)
7. M. Mambrini, A. Läuchli, D. Poilblanc, and F. Mila, Plaquette valence-bond crystal in the frustrated Heisenberg quantum antiferromagnet on the square lattice, *Phys. Rev. B* 74(14), 144422 (2006)
8. R. F. Bishop, P. H. Y. Li, R. Darradi, J. Schulenburg, and J. Richter, Effect of anisotropy on the groundstate magnetic ordering of the spin-half quantum J_1^{XXZ}-J_2^{XXZ} model on the square lattice, *Phys. Rev. B* 78(5), 054412 (2008)
9. R. Darradi, O. Derzhko, R. Zinke, J. Schulenburg, S. E. Krüger, and J. Richter, Ground state phases of the spin-1/2 J_1-J_2 Heisenberg antiferromagnet on the square lattice: A high-order coupled cluster treatment, *Phys. Rev. B* 78(21), 214415 (2008)
10. V. Murg, F. Verstraete, and J. I. Cirac, Exploring frustrated spin systems using projected entangled pair states, *Phys. Rev. B* 79(19), 195119 (2009)
11. J. Richter and J. Schulenburg, The spin-1/2 $J1$ t $J2$ Heisenberg antiferromagnet on the square lattice: Exact diagonalization for N=40 spins, *Eur. Phys. J. B* 73(1), 117 (2010)
12. J. Reuther and P. Wölfle, J_1-J_2 frustrated two-dimensional Heisenberg model: Random phase approximation and functional renormalization group, *Phys. Rev. B* 81(14), 144410 (2010)
13. H. C. Jiang, H. Yao, and L. Balents, Spin liquid ground state of the spin-1/2 square J_1-J_2 Heisenberg model, *Phys. Rev. B* 86(2), 024424 (2012)
14. L. Wang, D. Poilblanc, Z. C. Gu, X. G. Wen, and F. Verstraete, Constructing a gapless spin-liquid state for the spin-1/2 J_1-J_2 heisenberg model on a square lattice, *Phys. Rev. Lett.* 111(3), 037202 (2013)
15. W.-J. Hu, F. Becca, A. Parola and S. Sorella, Direct evidence for a gapless Z_2 spin liquid by frustrating Néel antiferromagnetism, *Phys. Rev. B* 88(6), 060402(R) (2013)
16. S. S. Gong, W. Zhu, D. N. Sheng, O. I. Motrunich, and M. P. A. Fisher, Plaquette ordered phase and quantum phase diagram in the spin-1/2 J_1-J_2 square Heisenberg model, *Phys. Rev. Lett.* 113(2), 027201 (2014)
17. A. Metavitsiadis, D. Sellmann and S. Eggert, Spin-liquid versus dimer phases in an anisotropic J_1-J_2 frustrated square antiferromagnet, *Phys. Rev. B* 89(24), 241104(R) (2014)
18. J. Richter, R. Zinke, and D. J. J. Farnell, The spin-1/2 square-lattice J_1-J_2 model: The spin-gap issue, *Eur. Phys. J. B* 88(1), 2 (2015)
19. A. F. Barabanov, A. V. Mikheyenkov, and N. A. Kozlov, Quantum phase transition in a frustrated two-dimensional magnetic system: A matrix projection approach, *JETP Lett.* 102(5), 301 (2015)
20. S. Morita, R. Kaneko, and M. Imada, Quantum spin liquid in spin 1/2 J_1-J_2 Heisenberg model on square lattice: Many-variable variational Monte Carlo study combined with quantum-number projections, *J. Phys. Soc. Jpn.* 84(2), 024720 (2015)
21. T. P. Cysne and M. B. Silva Neto, Magnetic quantum phase transitions of the two-dimensional antiferromagnetic J_1-J_2 Heisenberg model, *Europhys. Lett.* 112(4), 47002 (2015)

22. C. A. Lamas, D. C. Cabra, P. Pujol, and G. L. Rossini, Path integral approach to order by disorder selection in partially polarized quantum spin systems, *Eur. Phys. J. B* 88(7), 176 (2015)
23. K. Majumdar and T. Datta, Zero temperature phases of the frustrated J_1-J_2 antiferromagnetic spin-1/2 Heisenberg model on a simple cubic lattice, *J. Stat. Phys.* 139(4), 714 (2010)
24. A. F. Barabanov, V. M. Beresovsky, and E. Žąsinas, Quantum phase transitions in a three-dimensional frustrated $S = 12$ Heisenberg antiferromagnet, *Phys. Rev. B* 52(14), 10177 (1995)
25. D. J. J. Farnell, O. Götze, and J. Richter, Ground-state ordering of the J_1-J_2 model on the simple cubic and body-centered cubic lattices, *Phys. Rev. B* 93(23), 235123 (2016)
26. J. R. Viana, J. R. de Sousa, and M. A. Continentino, Quantum phase transition in the three-dimensional anisotropic frustrated Heisenberg antiferromagnetic model, *Phys. Rev. B* 77(17), 172412 (2008)
27. C. Pinettes and H. T. Diep, Phase transition and phase diagram of the J_1-J_2 Heisenberg model on a simple cubic lattice, *J. Appl. Phys.* 83(11), 6317 (1998)
28. Y. Iqbal, R. Thomale, F. Parisen Toldin, S. Rachel, and J. Reuther, Functional renormalization group for three-dimensional quantum magnetism, *Phys. Rev. B* 94(14), 140408(R) (2016)
29. J. Oitmaa, Frustrated J_1-J_2-J_3 Heisenberg antiferromagnet on the simple cubic lattice, *Phys. Rev. B* 95(1), 014427 (2017)
30. F. Ma, Z. Y. Lu, and T. Xiang, Arsenic-bridged antiferromagnetic superexchange interactions in LaFeAsO, *Phys. Rev. B* 78(22), 224517 (2008)
31. A. S. T. Pires, Anisotropic easy axis $S = 1$ antiferromagnetic Heisenberg model with competitive interaction on a square lattice, *Solid State Commun.* 193, 56 (2014)
32. H.Y. Wang, Green's Function in Condensed Matter Physics, Alpha Science International Ltd. and Science Press, Beijing, 2012
33. J. Oitmaa, C. J. Hamer, and W. Zheng, Heisenberg antiferromagnet and the XY model at $T = 0$ in three dimensions, *Phys. Rev. B* 50(6), 3877 (1994)
34. A. W. Sandvik, Critical temperature and the transition from quantum to classical order parameter fluctuations in the three-dimensional Heisenberg antiferromagnet, *Phys. Rev. Lett.* 80(23), 5196 (1998)
35. H. Y. Wang, L. J. Zhai, and M. Qian, The internal energies of Heisenberg magnetic systems, *J. Magn. Magn. Mater.* 354(3), 309 (2014)
36. P. Fröbrich and P. J. Kuntz, Many-body Green's function theory of Heisenberg films, *Phys. Rep.* 432(5–6), 223 (2006)
37. T. Holstein and H. Primakoff, Field dependence of the intrinsic domain magnetization of a ferromagnet, *Phys. Rev.* 58(12), 1098 (1940)